

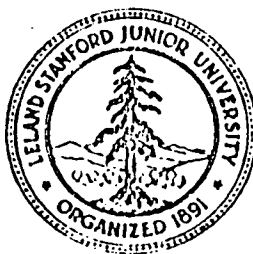
N84-26559

C S S A

HARD X-RAY AND MICROWAVE MORPHOLOGY

by

Vahé Petrosian



CENTER FOR SPACE SCIENCE AND ASTROPHYSICS
STANFORD UNIVERSITY
Stanford, California

HARD X-RAY AND MICROWAVE MORPHOLOGY

by

Vahé Petrosian

CSSA-ASTRO-84-08

February 1984

National Aeronautics and Space Administration
Grant NSG-7092

National Science Foundation
Grant ATM 82-18125

Center for Space Science and Astrophysics
Stanford University
Stanford, California

FOREWORD

This report was the outcome of the series of three SMM workshops held at NASA Goddard Space Flight Center, Greenbelt, MD, in 1983 and 1984. It is a report of a subgroup of the transport group (C) of the workshop. The task of the subgroup, headed by the author, Vahé Petrosian, was an in depth analysis of data (and comparison with observation) from SMM and Hinotori on the Hard X-ray and Microwave Morphology of the flares. The author was aided in the gathering of the relevant data by Drs. Mukul Kundu and Shinjo Enomé, who are not responsible for any errors in the report and may not agree with all the theoretical interpretations presented here.

This work was supported in part by NASA Grant NSG 7092 and NSF Grant ATM 82-18125.

HARD X-RAY AND MICROWAVE MORPHOLOGY

1. Observations

The strong correlation in the temporal evolution of hard x-rays and microwave radiation established over the years has led to the belief that the same or very closely related populations of electrons are responsible for both of these flare radiations. High spatial resolution observations at both wavelength ranges provides further information on the details of this correlation.

Since the first fanbeam observation of flares by Enome et al (1969) with resolution 24" at 9.4 GHz, the new instruments, such as the NRAO 3 element interferometer with resolution 10" at 2.7 GHz (Alissandrakis and Kundu 1975), the WSRT array with one dimensional resolution of 6" at 5 GHz (Allissandrakis and Kundu 1978, Kattenberg and Allaart 1981) and finally the VLA with two dimensional resolution of 1" at 15 GHz (Marsh et al 1980, Lang et al 1981 and Kundu et al 1981) have steadily improved the resolution of the microwave observation. VLA observations (Kundu et al 1982, Dulk et al 1983) and fanbeam observations at 35 GHz (Nagoya) and 17 GHz (Noboyama) have continued while the HXIS on SMM and the SXT on Hinotori have begun for the first time to provide spatially resolved images with resolution of about 10" at x-ray energies of less than 40 keV. Unfortunately, only for a very few flares there exists high resolution images simultaneously at both microwave and hard x-rays. Consequently, we must still rely on the data of more numerous events with only hard x-ray or microwave images.

We first summarize the results of observations where there exists only high resolution microwave data, then those with only x-ray data and, finally, the few cases with both x-ray and microwave observations.

a. Microwaves

The early studies of spatial structure of microwave radiation from flares were summarized by Marsh and Hurford (1981) and the more recent results by Kundu (1983). It should be noted at the outset that, unlike the x-ray studies, the microwave observations (in particular the high resolution one-dimensional results from WSRT and the two-dimensional results from the VLA) have not been as systematic, continuous and carried over as long a period as the x-ray observations. This is because such large telescopes are not necessarily dedicated only to solar flare observations. Consequently, it is difficult to classify the microwave structure in well defined categories. In spite of this, these observations have shown some common features which we will concentrate on here, remembering that there may be more complex structures yet to be studied, analyzed and classified.

The most general statement that can be made is that the brightest point of the microwave radiation during the impulsive phase occurs near a magnetic neutral line and not on an H-alpha kernel, and that in cases with simple field geometries there is a single dominant source. Whenever a secondary source is detected, that source also lies near another neutral line (e.g., May 26, 1980, flare, Kundu 1983). It can be concluded that the predominant microwave emission does not come from the footpoints of the flaring loop. In some flares the microwave source is approximately midway between the footpoints and is nearly equally but oppositely polarized (circular) on both sides of the maximum brightness spot (see Figure 1). The simplest interpretation of these observations is that the emission comes from the top of a loop. Variation with frequency of observation of the structure and polarization then tell us something about the geometry of the loop and the pitch angle distribution of the radiating electrons (Petrosian 1982). However, there are flares where

only one sense of polarization is observed (see Fig. 2 and cf. Kundu 1983), and there are cases where the source is not located very high up in the corona (Kai et al 1982). These features have been attributed to asymmetric magnetic loops (Kundu and Vlahos 1979), but, as we shall discuss below, such structures could also arise when a non-circular or sheared loop is viewed from an angle away from the line perpendicular to the field at the top of the loop.

b. X-ray Morphology

Prior to the data from SMM and Hinotori spacecraft, the only information on spatial structure of hard x-rays was obtained from stereoscopic observation by PVO and ISEE-3 satellites (Kane et al 1979). These observations do not provide images but give information on the height of the hard x-ray emitting regions. On the other hand, they extend to much higher x-ray energies than the imaging instruments and tell something about the variation with height of x-ray spectra, which turns out to be very useful in the modeling of flares (Leach and Petrosian 1983).

The first hard x-ray images of flares were obtained by the HXIS on SMM. The analysis of the few early flares emphasized x-ray structure consisting of two sources which were identified as the footpoints of flaring loops (Hoyng et al 1981). But as indicated by Duijveman and Hoyng (1983), there are many flares where the bulk of the hard x-rays (>16 keV) come from a single source.

However, the analysis of the data from SXT on Hinotori, which are published in the Proceedings of the Hinotori Symposium on Solar Flares (Ohki et al 1982, Tsuneta et al 1982, and Takakura et al 1982) and of the U.S.-Japan Seminar published in Solar Physics (Ohki et al 1983, Tsuneta et al 1983, Takakura et al 1983 and Kosugi et al 1983) seems to emphasize the predominance of the flare images consisting of a dominant single source which sometimes expand and become elongated, and sometimes shrink. There is also rarer occurrences of double sources (not necessarily of equal intensity) which

emerge into a single source located between the original two sources as the flare progresses. More recent analyses of HXIS show similar structures and evolution (Machado 1983, and Machado et al 1983).

Based on SXT data and data on the light curves and spectral changes from other instruments on board Hinotori, various classifications of the flares have been given by Ohki et al (1982), Tanaka (1983), Tanaka et al (1983) and Tsuneta (1983). No such classification is given for the HXIS data. We note that these classifications are based on the strongest flares which may not be representative of all flares, the majority of which are weaker and shorter lived than the ones used for this classification. It should also be noted that they are based on qualitative differences between spatial structures, spectra and the so-called impulsiveness of the light curve. For a more thorough analysis the parameters describing these characteristics should be quantified and flares binned accordingly. The flares studied may be the extreme cases so that further analysis may show a continuum of classes with no clear dividing line between the present categories.

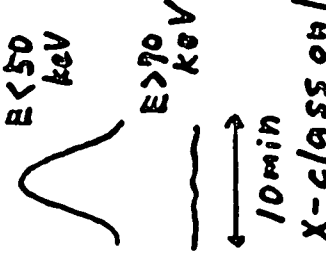
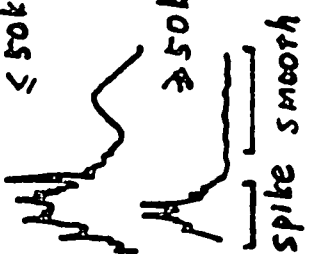
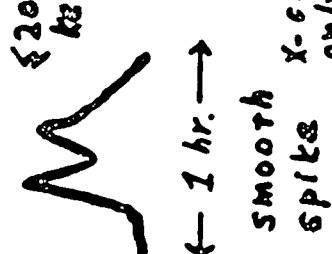
The Hinotori data is classified into three types, A, B and C, as described in Table 1.

Type A events are defined as those which have a smooth light curve below 40 keV (no discernable spiky features; note that spikiness is not quantified), soft spectrum (spectral index > 6 for a power law fit but it may also be fitted by an exponential spectrum) and consist of a single compact source. Two examples of such flares have been extensively studied (Tsuneta et al 1984) which are the April 2nd and July 17th flares of 1981. The April 2nd flare (Figure 3) shows a single steady point source (perhaps barely resolved at 15"). Strong Fe XXVI lines are also observed throughout these events.

Type B flares are those with two distinct hard x-ray bright spots during

Table 1

Hinotori Classification of Solar Hard X-ray Bursts

Type	Time Profile	Hard X Spectrum	Hard X ($E > 15 \text{ keV}$) Image	Gamma-ray Timing
A	 <p>$E < 50 \text{ keV}$ $E > 70 \text{ keV}$ $\longleftrightarrow 10 \text{ min}$ X-class only</p>	<p>Very soft $t \sim 7 \sim 9$ hot plasma $T \sim 3 \sim 5 \times 10^9 \text{ K}$ $E_H \sim 10^{49} / \text{cm}^3$ $\rightarrow \text{Fe XXVI}$</p>	<p>Small point-like ($\sim 10''$) low-altitude ($\leq 5000 \text{ km}$) $\longleftrightarrow 10 \text{ arcsec.}$</p>	<p>No γ-ray emission</p>
B	 <p>$E < 50 \text{ keV}$ $E > 50 \text{ keV}$ spike smooth</p>	<p>impulsive phase \rightarrow hard gradual phase \rightarrow soft</p>	<p>Double Sources Footpoints Coronal loop-like Hd hard X $\longleftrightarrow 10 \text{ min.}$</p>	<p>delay \leq several sec. No γ-ray emission</p>
C	 <p>$E < 200 \text{ keV}$ $\longleftrightarrow 1 \text{ hr.}$ smooth spikes only</p>	<p>power-law $t \sim 3 \sim 5$ $\left(\frac{d\dot{E}}{dE}\right) < 0$</p>	<p>High-altitude coronal source (stationary) Hd hard X $\longleftrightarrow 1 \text{ min.}$</p>	<p>delay \sim tens of sec \sim min.</p>

the initial (impulsive) part of the flare which evolve into a single source located somewhere in between the initial bright regions. Along with this evolution it is observed that spikiness of the light curve disappears and the spectrum softens. Hinotori events of July 20 (Figure 4) and Oct. 15 of 1981 are two such events.

Finally, there are the type C flares which, like the Type A flares, consist of a single source, but the source is more diffused and is clearly displaced from the H-alpha kernel and, like the microwave sources described above, could be emanating from the top of a loop. The light curve is also smooth even at energies greater than 40 keV and the spectrum is hard. The May 13 (Figure 5) and April 27 flares of 1981 are two such events.

As mentioned above, HXIS also shows flares with spatial structures similar to those described by Hinotori. Figure 6 shows some such examples.

It should be noted that some of the type A flares may be unresolved type B events which are either intrinsically more compact or are elongated sources viewed along the major axis.

c. Hard X-rays and Microwave Morphologies

There are less than a dozen flares which are resolved (in one-dimensional scan or in two-dimensional mapping) at both hard x-ray and microwave energies. Here we describe the brightest of these and concentrate on the relation between the hard x-ray and microwave structure of the most important features.

Hinotori Events. We summarize here four events representing all the three types described above.

The August 11, 1981, flare is classified as type A but as far as the x-ray image is concerned, it falls on the border line between types A and C. Without a quantitative measure of the distinguishing parameters of the various types, one cannot resolve this ambiguity. In any event, the x-ray image appears to be a steady single elongated source (hint of a double source at the

rising phase). The one-dimensional 17 GHz tracing shows a near coincidence of the peak microwave and x-ray positions (Figure 3). Both maxima seem to be located over a neutral magnetic line. (For details see Takakura et al 1983.)

April 1 and May 13, 1981, flares are both classified as type C. May 13 has a very smooth time profile even above 100 keV, while the x-ray light curve for the April 1 flare is midway between the August 11 and May 13 flares. As shown in Figures 5 and 7, the 35 GHz microwave position agrees with the position of single dominant x-ray source. Both emissions appear to come from the top of a loop or arcade of loops. However, there is some asymmetry in the one-dimensional microwave image. This asymmetry becomes stronger (indicating existence of two sources) in the later phases of the flare, and in the case of the April 1 event (Figure 7) it may be interpreted as a double source. Unfortunately, there is no x-ray image for these periods.

The Oct. 15, 1981, flare may be classified as type B because initially it consists of two sources (one much brighter than the other). However it is not clear if these sources correspond to any H-alpha kernels. The 35 GHz image can be decomposed into a double source with the stronger microwave corresponding with the weaker x-ray source (Figure 8). There is a secondary peak in the light curve during which the x-ray structure changes rapidly. The brighter source moves about 30 arc sec south-ward and the weak source becomes stronger. Finally, during the decaying phase these sources disappear and a third source appears in a new position. There are no microwave images for the second peak or the decay phase of this flare. Most probably this is a type B flare like the July 20, 1981, limb flare. However, one cannot rule out the less likely possibility that the four different bright regions correspond to the top of four different loops.

SMM Events. We now describe four SMM events which have also been

observed either by the WSRT or the VLA.

Nov. 5, 1980, event (Figure 9) described by Hoyng et al, 1983, has excellent overlapping HXIS and VLA coverage. The 15 GHz radiation appears to conform to the standard picture described above, consisting of one source (oppositely polarized on both sides) located above a neutral line. The light curves at hard x-rays and at 9.4 GHz show a type B profile and consist of three peaks, with the third peak being a gradual one. (In the VLA observation at 15 GHz the first two peaks are unresolved and the third peak is not discernable.) The 16 to 30 keV HXIS counts in various pixels conform to the type B character of this event in that, initially, there is less flux from the region over the neutral line than from the H-alpha bright spots, and during the second and third peaks most of the x-rays come from the approximate center of gravity of the bright region and coincide with the bright microwave source.

July 13, 1980, event described by Kattenberg et al (1984) shows two sources in coincidence with the H-alpha bright patches. Unlike the type B flares there is no gradual peak (or phase) in the light curve and no emergence of a single source in the middle. Unfortunately, the baseline of the WSRT one-dimensional microwave tracing is perpendicular to the line connecting the two x-ray sources so that we do not know if the microwave source is also double. However, the usual centrally located microwave image is consistent with the data.

On June 24, 1980, two bursts at 15:20 and 19:57 UT were extensively mapped at 6 cm by the VLA with somewhat weak coverage by the HXIS on SMM (Kundu et al 1983). The 15:20 event shows a hard x-ray image displaced by 20 to 30 arc sec from the microwave source which is a typical bipolar (separated right and left circularly polarized structures as in Figure 1) source. The softer x-ray and microwave emissions are co-spatial, presumably coming from the loop top while the hard x-rays may come from a footpoint. This may

therefore be a type B event. The microwave source during the 19:57 burst is complex, consisting initially of two oppositely oriented bipolar sources. During the peak of hard x-ray burst a third (perhaps another bipolar) source appears in between the previous two sources. One can interpret these as consisting of three loops, the first two of which give little hard x-rays while the third produces some weak hard x-ray emission.

d. Summary

The sample of flares described above is obviously incomplete in many ways. In general, any sample is limited by the selection effects associated with observing instruments. However, certain aspects of the flare phenomenon are affected less than others by such selection criteria. We hope that by concentrating on the gross features of the flare phenomenon the influence of the selection effects can be minimized. The following is a summary of the prominent features of x-ray and microwave morphology.

1) There is no direct evidence for microwave emission from the footpoint of the loop presumably located on the H-alpha bright patches. Whenever such a comparison can be made the microwave emission comes from a region above the neutral line in between the H-alpha bright patches. Note, however, that there are exceptions where a minor microwave feature may be near an H-alpha bright patch (Dulk et al 1983) and that the bursts where one sense of circular polarization is dominant have been interpreted as emission from one footpoint of an asymmetric loop.

2) In the majority of cases the x-ray emission comes from a single dominant source (types A and C), which is found to be located above a neutral line and not on an H-alpha bright patch, except that for some compact, type A bursts higher resolution is needed for confirmation of this picture. The structure of type B bursts with two bright x-ray sources (normally coincident

with H-alpha patches) evolves into a single source located in between the H-alpha patches.

3) The limited hard x-ray and microwave data obtained so far are consistent with, but are not a direct evidence for, the conclusion that such large scale changes in the images occur on a hydrodynamic time scale, with velocity $v \approx 50$ to 200 km/sec.

4) The hard x-ray and microwave images, even though different in detail, have roughly the same location whenever both images are dominated by a single source. For bursts with initial double x-ray images, the emerging single source most probably coincides with the microwave sources presumably located near the top of a loop.

As we shall show in the next section, the above general features are consistent with the non-thermal model, whereby semi-relativistic electrons are injected in a closed loop somewhere in the corona. One aim of such observation and the theoretical work is to determine the constraint the observations provide on the model parameters such as the field geometry, loop size and density and the spectrum and pitch angle distribution of the accelerated electrons.

2. Interpretation

We now interpret the above data in the framework of the non-thermal models whereby electrons accelerated to energies well beyond the thermal energy of the coronal plasma are injected in the solar atmosphere. These models are variously classified as thick target, thin target, trapped, etc.

The traditional trapped models require both a rapid convergence of the field lines and a low density. For electrons to mirror back and forth in the corona, one needs $\delta B/B \gg \delta L/\lambda$ where L is a length scale and λ is the mean free path of the electrons. And for the x-ray producing electrons to

survive for the whole duration of the impulsive phase ($> \text{few seconds}$) one needs density $n < 10^8 \text{ cm}^{-3}$.

The thin target model will be realized only in an open magnetic field configuration. The isotropic or outward streaming injections of electrons can be dismissed because, contrary to observations, they require an equal number of electrons reaching the earth as are needed to produce the hard x-rays. If the electrons are highly beamed toward the chromosphere, the result will be similar to the thick target, closed field configurations discussed below.

Consequently, we will consider only the general thick target model where electrons are injected in a closed magnetic loop (Figure 10). We shall need to specify the site of injection of the electrons. If the site of injection is very deep, well below the transition zone (point 1 of Figure 10a), the electrons lose energy quickly, causing direct heating and evaporation of chromospheric plasma, and produce hardly any hard x-rays above the transition region. We shall not discuss this possibility here because it will fail to describe type C bursts discussed above. On the other hand, if the injection is at lower densities (point 2) so that all of the outgoing particles eventually reach the top of the loop, then the situation is qualitatively similar to the injection at the top of the loop (point 3) which is what we shall assume.

a. Transport of Electrons

The transport of the non-thermal electrons is affected by many parameters. In particular, if the pitch angle distribution of the electrons is highly anisotropic (beamed electrons), they are subject to some instabilities which change the distribution on a time scale of the order plasma oscillations. We shall not consider such cases here. Furthermore, if the beams constitute a high current, then a reverse current is set up. The electric field which drives the reverse current also decelerates the original

beam. These aspects of the transport are discussed in Section III.A. Here we concentrate on the collisional effects and the role of large scale static magnetic fields.

We present here a brief summary from Leach and Petrosian (1981), LP I, who solve the transport of electrons using the Fokker-Planck method. The solar flare plasma conditions allow for various simplifying assumptions so that the differential equation describing the distribution of electrons $f(E, \mu, \tau)$, where $f dE d\mu d\tau$ is the number density in the energy range dE (in units of mc^2), pitch angle cosine range $d\mu$ and dimensionless column depth range $d\tau = dN/N_0$ ($N_0 = 5 \times 10^{22} \text{ cm}^{-2}$ is the column depth required for stopping of an electron with $E = 1$) is

$$\mu \frac{\partial f}{\partial \tau} = (1 - \mu^2) \frac{d \ln B}{2 d \tau} \frac{\partial f}{\partial \mu} + \frac{1}{\beta} \frac{\partial}{\partial E} \left(\frac{f}{\beta} \right) + \frac{1}{\beta^4 \gamma^2} \frac{\partial}{\partial \mu} \left[(1 - \mu^2) \frac{\partial f}{\partial \mu} \right] \quad (1)$$

Here $d \ln B / d \tau$ describes the variation of the magnetic field along the loop and $\gamma = 1 + E = (1 - \beta^2)^{-1/2}$. The three terms on the right hand side account for the magnetic mirroring, collisional energy losses and collisional diffusion in pitch angle⁺, respectively. As evident, given $d \ln B / d \tau$, the energy spectrum and pitch angle distribution are only a function of the column depth τ and the parameters describing the distribution at the point of injection, which is taken to be at $\tau=0$ at the top of the loop.

⁺ Note the difference between coefficient of the last term here and that given in LPI. For more details the reader is referred to the Leach (1984) Ph.D. Thesis, Stanford University. The difference is insignificant at non-relativistic energies and for hard x-rays considered below and by LPI.

Let us first consider uniform loops; $d\ln B/d\tau = 0$. Then, for small pitch angles α so that $\mu = 1 - \alpha^2/2$ the above equation can be solved analytically which, in terms of particle flux, $F = \beta cf$, for a power law energy spectrum and a gaussian pitch angle distribution at injection, $F(E, \mu, \tau=0) = F_0(E; \mu) = A E^{-\delta} e^{(\mu^2-1)/\alpha_0^2}$, gives

$$F(E, \mu, \tau) = A (\zeta^{1/2} E)^{-\delta} \zeta^{-x} [2/(\alpha_0^2 + \ln \xi)] e^{-[\alpha^2/(\alpha_0^2 + \ln \xi)]} . \quad (2)$$

For non-relativistic energies $\zeta = \xi = (1 + \tau/E^2)$ and $x = 1/2$. For extreme relativistic energies $\zeta = (1 + \tau/E)$, $x = 0$, and $\ln \xi = 4\tau/\zeta E^2$. As shown in LPI this approximate analytic expression provides a good description even for moderate pitch angles.

As evident, for $\tau/E^2 < 1$ [actually for the general case for $\tau(E+1)/E^2 < 1$], $\zeta = 1$ and the distribution is similar to that at $\tau = 0$, but as soon as τ/E^2 exceeds unity the number of particles with energy E starts to diminish rapidly and their pitch angle distribution broadens. For the loop as a whole then the mean pitch angle distribution is somewhere between the injected distribution and a broad (nearly isotropic) distribution at $\zeta \gg 1$. This means that models with widely different values of α_0^2 appear different only at the top of the loop but merge into indistinguishable nearly isotropic models lower down and on the mean their differences are smaller than one would suspect from the differences in the values of α_0^2 . Consequently, the radiation signature of spatially unresolved loops will tend to be closer to what one expects from an isotropic rather than a highly beamed pitch angle distribution. Note, however, that this is not true at relativistic energies (i.e. electrons producing the high frequency microwave radiation and the continuum gamma-rays). Such electrons lose energy more quickly than they diffuse in pitch angle.

The effect of magnetic field convergence, i.e., of a non-zero $d\ln B/d\tau$, is to mirror some of the electrons which do not reach to the chromosphere and confine them to the top of the loop. However, since the loop is not empty, such electrons also eventually scatter into smaller pitch angles and penetrate deeper and are thermalized. The over-all effect of the non-zero $d\ln B/d\tau$ is to isotropize the pitch angle distributions more quickly and enhance the effects described in the previous paragraph.

Briefly then, all non-thermal models relevant for the production of x-rays can be described by the general thick target model characterized by three parameters δ , the spectral index, α_0^2 , the pitch angle dispersion at injection and the flare plasma parameter $d\ln B/d\tau$ which has incorporated in it both field strength and density variation along the loop. Let us now consider the effects of these parameters on the observables.

b. Non-thermal Emission

Two aspects of observation of the impulsive phase will be considered here. The first will be the morphology of hard x-ray and microwave spatial structure summarized in part 1 of this Section. The second will deal with the observation of hard x-ray polarization reported by G. Chanan in the second workshop. In this part we will also touch upon the polarization of the microwave radiation.

We shall be concerned only with the most prominent aspects of these observations and try to interpret them in the framework of a simple (semi-circular) loop model described above (cf. Figure 10a). As we shall see, the geometry of the loop and the physical parameters of the plasma in the loop play a significant role (much more than realized or emphasized on previous treatments) in determining the characteristics of the various emissions. We recognize that the assumed field geometry is too simplified. Our purpose is to determine to what extent such a simple model can reproduce the gross

observational features. Modification toward more realistic models can presumably accommodate the details of the deviation of burst characteristics from the norm.

In this analysis we shall rely heavily on work by Leach and Petrosian (1983, abbreviated as LPII) and on Petrosian (1982, PI). For a more complete treatment of the x-ray emission, the reader is referred to the Ph.D. thesis of John Leach (Stanford University, 1984, LI). Following them we assume a semi-circular loop (with radius R) in the corona with variable magnetic field which becomes vertical and uniform in the chromosphere. The last simplification is not significant because the mean free path of the electrons decreases rapidly below the transition zone. We also assume that the density, n , of the pre-flare plasma in the loop is constant, equal to n_0 , in the corona and that it increases rapidly in the transition region. The important parameter for our consideration is the column depth from the top of the loop to the transition region, $N_{tr} = n_0 \pi R/2$ and the parameter $d \ln B / d\tau$ describing the variation of magnetic field along the loop.

(i) Image Morphology

Hard x-rays. We begin with the spatial structure of x-rays in the range 16 to 50 keV. The x-ray emission is obtained from the flux F (eq. 2) of the transport analysis and the bremsstrahlung cross section. At these energies the x-rays and the electrons producing them are non-relativistic, the radiation is nearly isotropic and the scaling (see parameter ζ of eq. 2) between energy E of electrons and column depth τ directly translates into a similar scaling between τ and the photon energy k (in units of $m_e c^2$). Figure 11 (from LI) shows the variation of the x-ray intensity (normalized photon counts per energy interval dk and depth interval $d\tau$) with k and τ for three models. This intensity is nearly constant for

low τ but it decreases rapidly at higher column depths. The transition between these two regions occurs at $\tau = k^2/(k+1) \approx k^2$ for non-relativistic energies. It turns out that the following simple semi-empirical relationship gives an extremely accurate description of this variation.

$$I(k, \tau) d\tau \approx k^{-\delta+1} (1 + \tau/k^2)^{-\delta/2} d\tau/k^2. \quad (3)$$

This simple picture becomes complicated when we translate it into observables. Let us consider the circular loop of figure 10 as viewed directly from above. For comparison with observation we need the variation of the intensity projected on the solar disk $I(k, r)$ with the projected distance r from the center of the loop.

$$I(k, r) = I(k, \tau) d\tau/dr = I(k, \tau) (n_0/N_0) (1 - r^2/R^2)^{-1/2}. \quad (4)$$

The last geometric term plays a significant role as shown in Figure 12a. Note, however, that even for non-circular geometry $d\tau/dr$ increases rapidly as the footpoints are approached.

Now at a given energy k if the column depth N_{tr} is small, or more precisely if the dimensionless depth $\tau_{tr} = \tau(r=R) = N_{tr}/N_0 \ll k^2$, then $I(k, \tau)$ will be nearly constant for $0 < r < R$ and will be zero beyond R . However, because of the projection effects $I(k, r)$ will rise with r , such that the footpoints at $r = R$ will appear brighter than the top of the loop at $r = 0$. For $N_{tr} \gg k^2 N_0$ the brightness will decrease steadily from the top to the footpoints (cf. Figure 12b). The changeover of the location of the maximum brightness from $r = 0$ to $r = R$ will occur quickly around $N_{tr} = N_0 k^2 = 10^{20} \text{cm}^{-2} (k/22 \text{keV})^2$.

At energies less than 10 keV ($k < .02$) a low pre-flare value of $N_{tr} = 10^{19} \text{cm}^{-2}$ is sufficiently high to ensure that the maximum brightness at these energies occurs at the top ($r = 0$) of the loop. But such a low value of N_{tr}

is not sufficient to confine higher energy (say > 22 keV) electrons to the top of the loop. Such electrons will penetrate below the transition region so that their radiation at 22 keV will be concentrated on the footpoints. Only if N_{tr} is greater than 10^{20} cm^{-2} , then the top of the loop becomes brighter than the footpoints at these energies also.

This general picture is nearly independent of the viewing angle and the field geometry because as mentioned, in general, $d\tau/dr$ does become very large near the footpoints. However, the details of the shapes of the curves drawn on Figure 12 do depend on the field geometry and the viewing angle.

This behavior, therefore, suggests that for the large, diffuse C type flares described in the first part of this section, $N_{tr} > 10^{20} \text{ cm}^{-2}$ (perhaps $n \sim 10^{10} \text{ cm}^{-3}$, $L \sim 10^{10} \text{ cm}$) so that one sees the confinement of the 10 to 40 keV photons to the tops of the loop. While, on the contrary, for the type B events observed by HXIS and Hinotori, initially $N_{tr} < 10^{20}$ and the emission is concentrated on the footpoints. The asymmetry of the radiation from the two footpoints as commonly observed must then be attributed to an asymmetric non-circular sheared field geometry (e.g., Figure 10b). As observed by Hinotori (Figure 4) and in some events by HXIS (Figure 6), the double images merge into a single coronal source as the flare progresses. This means that the column depth is increased from its initial low value to a value larger than 10^{20} cm^{-2} . As mentioned in connection with observations, such changes seem to occur on a hydrodynamic time scale suggesting that the evaporation of flare plasma may be the cause of the increase in the coronal column depth. The following order of magnitude calculation shows that this is a distinct possibility.

Let us assume that most of the energy $\mathcal{E} = \langle E \rangle \int F dt$ deposited by particles of mean energy $\langle E \rangle$ and flux F in a loop of cross sectional area A

goes into evaporation. If we further assume that the evaporated particles acquire the post flare temperature $kT \approx \text{keV}$, then equating the energy of the evaporated material with \mathcal{E} we find that $kT\Delta n LA = \langle E \rangle A \int F dt$ where L is the length of the loop. From this we find the change in the column depth $\Delta N = L\Delta n \approx (\langle E \rangle / \text{keV}) \int F dt$. For example, for $\langle E \rangle \approx 20 \text{ keV}$ an integrated flux $\int F dt \approx 5 \times 10^{18} \text{ cm}^{-2}$ is needed to increase the coronal column depth to the extent demanded by the observations.

Thus, it appears that the simple picture presented above can account for the variety of observed images and that with evaporation the temporal evolution of the images can also be accounted for. We note here that if the evaporated plasma is hotter than keV it will also contribute thermal x-rays at the low hard x-ray energies under consideration here. Further data will certainly be helpful in specifying the details of the models.

Microwaves. As discussed in part one of this Section, for the majority of observed bursts the most likely location of the microwave source is at the top of the loop. However, the explanation for this observation is different than that presented above for hard x-rays. This is because the microwaves are the result of gyrosynchrotron emission by much higher energy electrons (E order of unity) which, unlike the lower energy hard x-ray emitting electrons, cannot be confined as easily. The confinement to the top of the loop of such high energy electrons will require N_{tr} well above 10^{22} cm^{-2} . This is obviously unlikely and some other explanation is needed for concentration of the microwave emission to the top of the loops.

Microwave producing electrons are clearly present throughout the whole loop but the efficiency of gyrosynchrotron emission varies throughout the loop and depends on the direction and strength of the B field. The gyrosynchrotron radiation is strongest in the direction perpendicular to the field line. This factor alone, i.e., assuming everything else is equal throughout the loop,

will favor a maximum brightness located in between the footpoints. For example, the simple loop of Figure 10a when viewed from above will be brightest at $r = 0$. Note that this aspect is, to the first order, independent of the viewing angle. However, the gyrosynchrotron emission depends also on the number of electrons and the strength of the magnetic field. At a given frequency ν the emission from stronger field regions corresponds to lower harmonics of gyrofrequency ν_b . The lower harmonics are produced by lower energy electrons (very roughly, $E \propto (\nu/\nu_b)^{1/2}$, cf. Petrosian 1982 for the exact relation) which are more numerous. Since the field strength only decreases with the height above the photosphere, emission from higher regions could dominate only if this variation is slow. Finally, the strength of the gyrosynchrotron emission is a function of the pitch angle distribution of the electrons. Only if the pitch angle distribution of the accelerated electrons is broad (i.e., if the parameter α_0^2 introduced in the discussion of equations (1) and (2) is not too small) will the emission from the coronal region be important. Otherwise, if electrons of energy $E \approx 1$ are beamed along the field line, they remain so throughout the corona and give little gyrosynchrotron radiation. The pitch angle distribution becomes broader and the radiation efficiency increases only below the transition region, i.e., at the footpoints. (For further details the reader is referred to PI.) Another factor which also aids the relative enhancement of emission from the coronal part of the loop is the fact that gyrosynchrotron radiation is subject to various absorption and suppression effects (cf. Ramaty and Petrosian 1972), all of which are more important in the chromosphere than in the corona.

(ii). Polarization

X-rays. In the second session of this workshop G. Chanan

described a new observation of x-ray polarization, Tramiel et al (1984). In contrast to earlier observation by Tindo and his collaborators (see e.g. Tindo et al 1976 and references there to their earlier work), these new measurements exhibit a low degree of linear polarization ($<5\%$). Such low polarization naturally will arise in the so-called thermal models or if the pitch angle distribution of the electrons is nearly isotropic. Earlier studies of non-thermal models (Haug 1972, Langer and Petrosian 1977, Bai and Ramaty 1978) which ignored the scattering of the non-thermal electrons naturally reported a high degree of linear polarization for beamed electrons. Even Brown's (1972) calculation, which includes the scattering in an approximate fashion but does not include the curved loop geometry of the models under consideration here, has indicated a higher degree of polarization than observed. As a result it has been assumed that a low observed degree of polarization will be a strong evidence against the non-thermal models.

As stressed by Tramiel et al (1984), there are observational effects which would reduce the degree of polarization. However, here we shall show that even ignoring such uncertainties the observed low degree of polarization does not militate against the non-thermal models. A detailed description which relies heavily on the LPI and LPII can be found in Leach, Emslie and Petrosian (1984).

The primary reason for a low degree of polarization is what we emphasized in part 2a above, which is that no matter how strong the anisotropy of the injected particles, the average pitch angle distribution of a thick target model is very broad. In addition, because the direction of the linear polarization varies along a loop, the integrated x-ray emission from the whole loop will have the characteristic of the emission from a highly broadened distribution and will show lower polarization than one would expect from the distribution of the injected electrons. Table 2 summarizes the effect of

the two model parameters (see discussion following equation 1), and Figure 13 compares the observation of Tramiel et al with three model calculations.

As evident a low degree of polarization can arise naturally from some non-thermal models. In particular, we would like to note the strong effect of spectral index on polarization (Table 2). This is because the degree of polarization increases rapidly as photon to electron energy ratio approaches unity ($k/E \rightarrow 1$). For steep spectra (δ large) the bulk of photons with energy k are produced by electrons of only slightly larger energies ($k/E \lesssim 1$). However, for harder spectra (δ small) the contribution of higher energy electrons (i.e., those with k/E considerably less than unity) increases, causing a reduction in the polarization.

Microwaves. The bipolar microwave structure, i.e., those with opposite polarization on both sides of the maximum brightness (cf. Figure 1) is a natural consequence of the simple loop geometry we have been discussing here. The circular polarization is given by (Petrosian and McTiernan 1983).

$$P_c = \cot\theta \left\{ \frac{3(1+\delta)v_b \sin\theta/v}{1+(v_b \sin^2\theta/v \cos\theta)^2} \right\}^{1/2}. \quad (5)$$

where θ is the angle between the line of sight and the magnetic field lines. As evident $P_c = 0$ at $\theta = \pi/2$ and increases with opposite sense away from $\theta = \pi/2$ where the total microwave intensity is at its maximum. The simple circular loop, therefore, agrees with the qualitative features of the observation. Clearly by altering the field geometry one can change the variation of P_c . In particular, for highly asymmetric loop (see e.g. Figure 10b) it is possible to break the above symmetry between right and left hand polarization to a degree so that one sense of polarization becomes dominant as in Figure 2. Note that this is qualitatively similar to the field geometry proposed by Kundu and Vlahos (1979). However, the details of their model and that presented here are quite different.

Table 2

The variation of the maximum percentage polarization at 16 keV with the spectral index δ and the pitch angle distribution dispersion parameter α_0^2 of the injected electrons. The magnetic field is assumed to be uniform ($d\ln B/d\tau = 0$).

	α_0^2			
δ	∞^\dagger	0.4	0.04	0.01
3	≤ 5	≤ 5	≤ 5	6
4	8	8	11	13
5	10	11	20	21
6	10	16	26	26

† Electrons injected isotropically at the top of the loop

REFERENCES

- Alissandrakis, C.E., Kundu, M.R. 1975, Solar Phys., 41, 119.
- Alissandrakis, C.E., Kundu, M.R. 1978, Ap.J., 222, 342.
- Bai, T. and Ramaty, R. 1978, Ap.J., 219, 705.
- Brown, J.C. 1972, Solar Phys., 26, 441.
- Duijveman, A., Hoyng, P., and Machado, M.E. 1982, Solar Phys., 81, 137.
- Duijveman, A. and Hoyng, P. 1983, Solar Phys., 86, 279.
- Dulk, G.A., Bastian, T.S., Hurford, G.J. 1983, Solar Phys., 86, 219.
- Enome, S. Kakimura, T., Tanaka, H. 1969, Solar Phys., 6, 428.
- Haug, E. 1972, Solar Phys. 25, 425.
- Hoyng, P., Duijveman, A., Machado, M.E., Rust, D.M., Svestka, Z., Boelee, A., de Jager, C., Frost, K.J., Lafleur, H., Simnett, G.M., Van Beek, H.F., and Woodgate, B.E. 1981, Astrophys. J. (Lett), 246, L155.
- Hoyng, P., Marsh, K.A., Zirin, H., and Dennis, B.R. 1983, Ap. J. 268, 865.
- Kai, K., Kosugi, T. and Nakajima, H., 1982, Solar Phys. 75, 331.
- Kattenberg, A., Allaart, M.A.F. 1981, Thesis, Utrecht.
- Kattenberg, A., Allaart, M.A.F., de Jager, C., Schadell, A., Schrijven, J., Shibasaki, K., Svestka, Z. and Von Tend. 1984, (preprint).
- Kawabata, K., Ogawa, H., Takakura, T., Tsuneta, S., Ohki, K., Yoshimori, M., Okudaira, K., Hirashima, Y., and Kondo, I. 1982, Proc. HINOTORI Symposium, eds. Tanaka, Y. et al, ISAS, Tokyo, p. 168.
- Kundu, M.R. 1983, Solar Phys., 86, 205.
- Kundu, M.R. and Alissandrakis, C.E. 1975, MNRAS, 173, 65.
- Kundu, M.R. and Alissandrakis, C.E. 1977, Bull. Am. Astron. Soc., 9, 328.
- Kundu, M.R., Schmahl, E.J., Rao, A.P. 1981, Astron. Astrophys., 94, 72.
- Kundu, M.R., Schmahl, E.J., Velusamy, T. 1982, Ap.J. 253, 963.
- Kundu, M.R. and Vlahos, L. 1979, Ap.J., 232, 595.
- Lang, K.R., Willson, R.F., Felli, M. 1981, Ap.J. 247, 338.
- Langer, S.H. and Petrosian, V. 1983, Ap.J., 215, 666.

- Leach, J., Emslie, A.G. and Petrosian, V. 1984, (submitted for publication).
- Leach, J. and Petrosian, V. 1981, Ap.J. 251, 781.
- Leach, J. and Petrosian, V. 1983, Ap.J. 269, 715.
- Machado, M.E. 1983, Solar Phys. 89, 133.
- Machado, M.E., Duijveman, A., Dennis, B.R. 1982, Solar Phys., 79, 85.
- Machado, M.E. Somov, B.V., Rovira, M.G. and deJager, C. 1983, Solar Phys. 85, 157.
- Marsh, K.A. and Hurford, G.J. 1980, Ap. J., 240, L111.
- Marsh, K.A. and Hurford, G.J. 1982, Ann. Rev. Astron. Astrophys., 20, 497.
- Marsh, K.A., Hurford, G.J., Zirin, H., Hjellming, R.M. 1980b, Ap.J., 242, 352.
- Ohki, K., Tsuneta, S., Takakura, T., Nitta, N., Makishima, K. Murakami, T., Ogawara, Y., Oda, M., and Miyamoto, S. 1982, Proc. HINOTORI Symposium, eds. Tanaka, Y. et al, ISAS Tokyo, p. 102.
- Ohki, K., Takakura, T., Tsuneta, S., and Nitta, N. 1983, Solar Phys., 86, 301.
- Petrosian, V. 1981, Ap.J., 251, 727.
- Petrosian, V. 1982, Ap.J., 255, L85.
- Petrosian, V. and McTiernan, J.M. 1983, Phys. Fluids, 26, 3023.
- Ramaty, R. and Petrosian, V. 1972, Ap.J. 178, 241.
- Takakura, T., Ohki, K., Tsuneta, S., Nitta, N., Makishima, K., Murakami, T., Ogawara, Y., and Oda, M., 1982 Proc. HINOTORI Symposium, eds. Tanaka, Y. et al, Tokyo, p. 142.
- Takakura, T., Ohki, K., Tsuneta, S., and Nitta, N. 1983a. Solar Phys., 86, 323.
- Tindo, I.P., Shuryghin, A.I. and Steffen, W., Solar Phys. 46, 219.
- Tramiel, L.J., Chanan, G.A. and Novick, R. 1984, Ap.J. (to be published).
- Tsuneta, S. 1983, Proc. France-Japan Seminar on Active Phenomena in the Outer Atmosphere of the Sun and Stars, in press.
- Tsuneta, S., Nitta, N., Ohki, K., Takakura, T., Tanaka, K., Makishima, K., Murakami, T., Oda, M., and Ogawara, Y. 1983a, Ap. J., submitted.
- Tsuneta, S., Takakura, T., Nitta, N., Ohki, K., Makishima, K., Murakami, T., Oda, M., and Ogawara, Y. 1983b, Solar Phys. 86, 333.

FIGURE CAPTIONS

1. VLA map at 15 GHz in right circular (black) and left circular (white) polarization superimposed on the H-alpha frames. The dashed line depicts the location of the magnetic neutral line (after Hoyng et al 1983).
2. Evolution in time of one dimensional map of the flare on 13 June 1980 at 6 cm with WSRT (3" resolution). Top: total intensity I, bottom circular polarization V. Note that the burst is polarized during the impulsive phase and only in one sense (after Kundu 1983).
3. Example of a type A flare of Aug. 11, 1981. The lower right hand panel shows a sketch of H-alpha flare at 01:55:45 UT and the direction of the peak of the one-dimensional brightness at 17 GHz and 01:45:10 UT. The other five panels show five different x-ray (25-50keV) images (after Takakura et al 1983).
4. Example of Type B flare, July 20, 1981: (a) impulsive phase, (b) gradual phase. Each image is 3' in size and each pixel is 6". The curved line bisecting the images shows the location of the solar limb. Note the evolution from a lower double to a higher single source (after Tsuneta et al 1983b).
5. Example of Type C flare May 13, 1981. Comparison of the hard x-rays (17 to 40 keV), the H-alpha photograph and the one dimensional radio images for the indicated times (after Tsuneta et al 1983b).
6. Examples from HXIS on SMM of double, single sources and evolving structures similar to those seen by Hinotori (after Duijveman and Hoyng 1983, and Machado 1983).

7. One dimensional microwave tracing and the hard x-ray image from SXT of the April 1, 1981, flare (after Kawabata et al 1983).

8. A comparison of the SXT hard x-ray image with the fanbeam radio brightness after the restoration for October 15, 1981, event (after Kawabata et al 1983). Whether the two images belong to footpoints of a single loop or emanate from top of the distinct loop is not known.

9. The microwave and hard x-ray images of November 5, 1980, flare. The lower panels are 8" x 16" in size and a dot indicates significant flux in excess of a single temperature fit (after Hoyng et al 1983).

10. Description of the geometry of loops: (a) semi-circular loop, (b) asymmetric sheared loop. Circled points (1), (2) and (3) refer to the possible locations of injection of electrons. The wavy arrows show the line of sight and the value of θ used in equation (5). Note that ds and $d\tau = n ds / N_0$ are measured from the point of injection, assumed to be at (3) along the loop. R is radius of the loop and r is a projected distance from the center of the loop.

11. Variation of the x-ray intensity $I(k, \tau)$ with photon energy k and column depth τ for three different models with spectral index $\delta = 5$ and pitch angle distribution parameter $\alpha_0^2 = 0.04, 0.4$ and 1 for curves labelled 5, 1 and 4, respectively (after Leach 1984). Equation (3) fits these numerically generated curves to better than 50 percent accuracy.

12. (a) Variation with projected distance (half of the loop) from the loop centers of various quantities. (b) Variation of expected hard x-ray brightness for the indicated values of $N_{tr}/N_0 k^2$.

13. A comparison between the polarization measured for flare 2I of Tramiet et al (1984) and the polarization calculated for three of the models of Leach and Petrosian (1983). For the solid line $\alpha_0^2 = 0.4$ and $d\ln B/d\tau = 0.0$, the dashed line $\alpha_0^2 = 0.4$ and $d\ln B/d\tau = 1.5 \times 10^{-9}$, and for the dotted line $\alpha_0^2 = 0.1$ and $d\ln B/d\tau = 1.5 \times 10^{-9}$. $d\ln B/d\tau = 1.5 \times 10^{-9}$ corresponds to a twentyfold increase in the magnetic field strength from the top of the loop to the transition region at $N_{tr} = 10^{19} \text{ cm}^2$. For a flare at disk center the viewing angle would be 0° ; for one on the solar limb it would be 90° (after Leach et al 1984.)

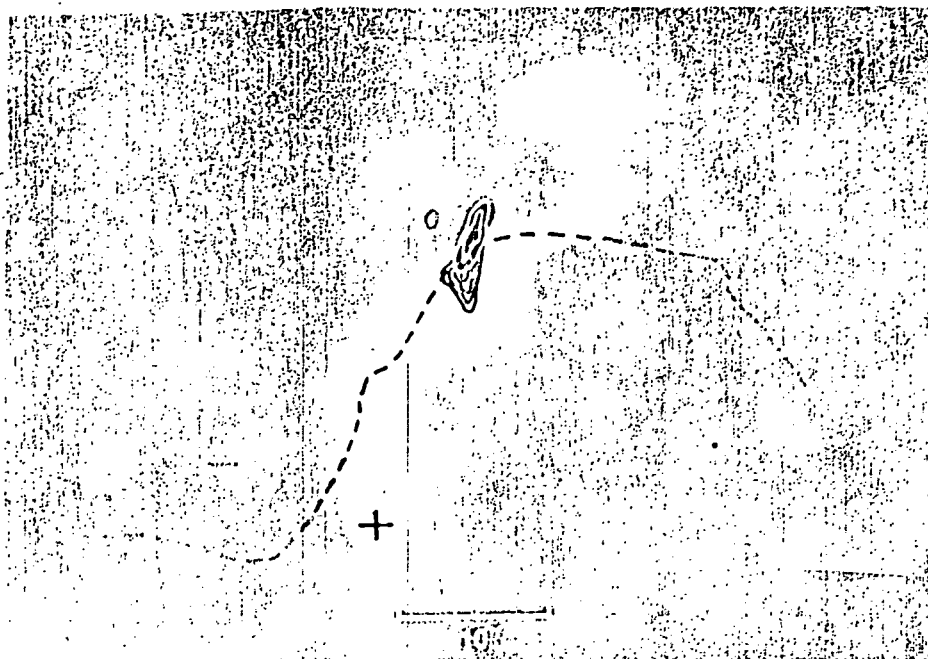


Figure 1

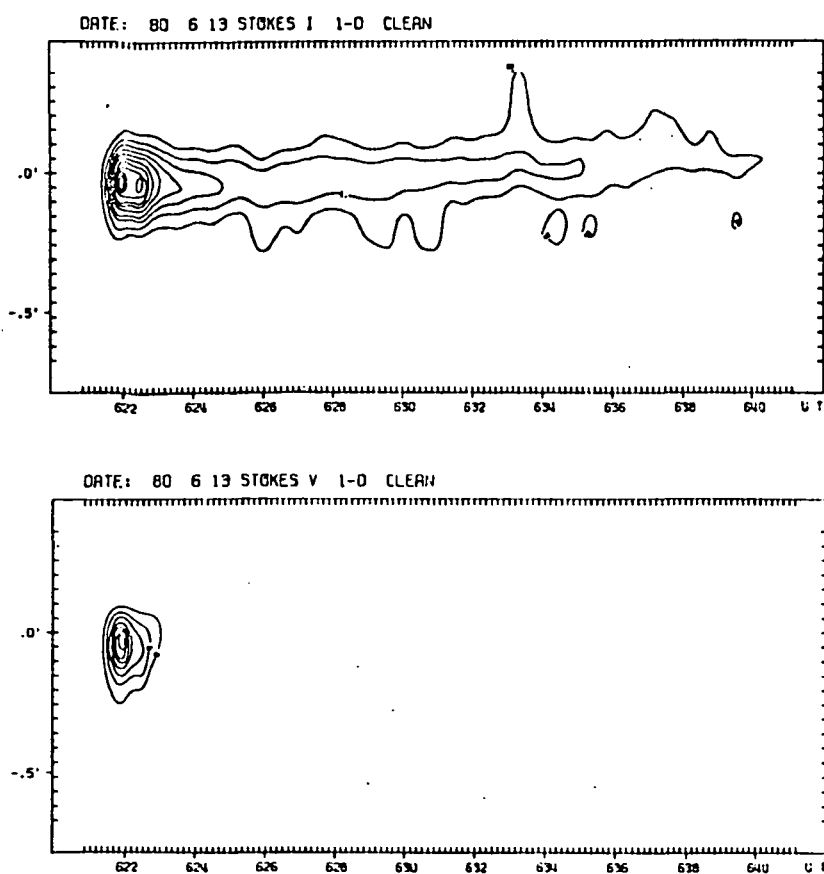


Figure 2

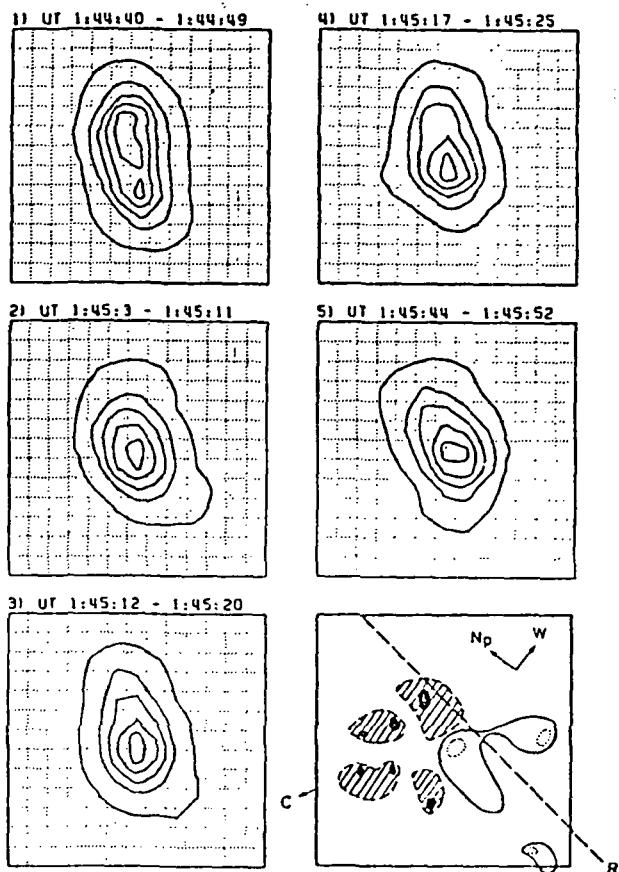


Figure 3

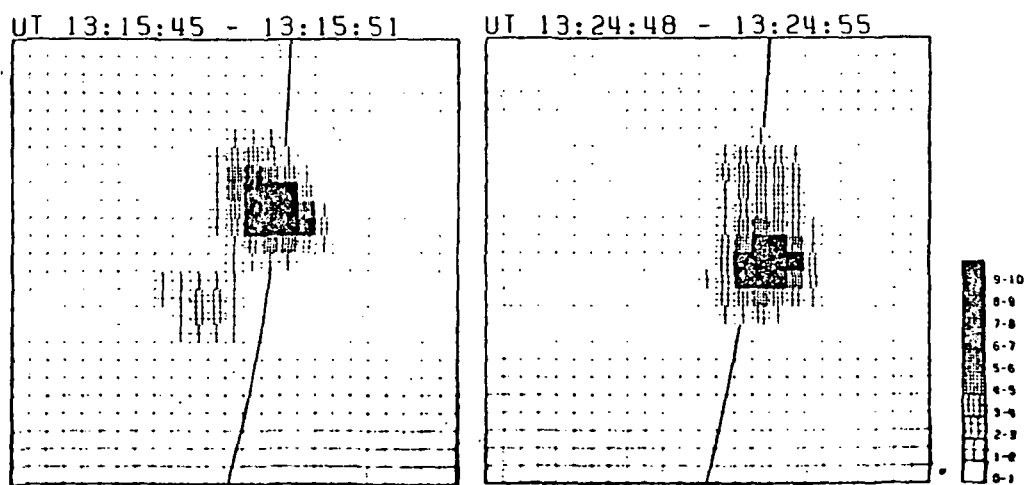
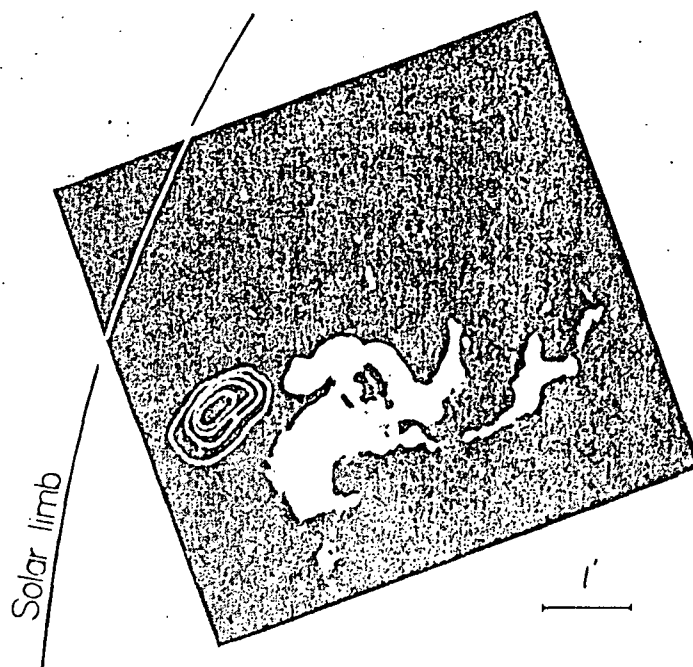


Figure 4

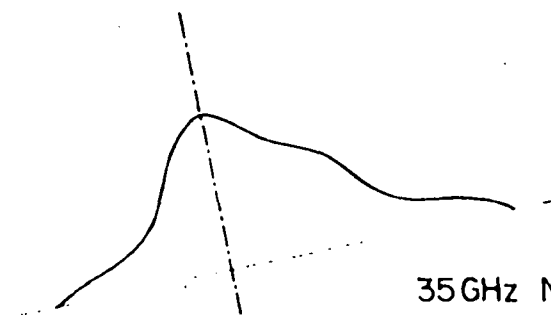
1981 MAY 13



E ————— W

Hard X-Ray : 04^H15^M(UT)

H α : 04 41 (UT)



35GHz Nagoya
04^H15^M05^S(UT)

Figure 5

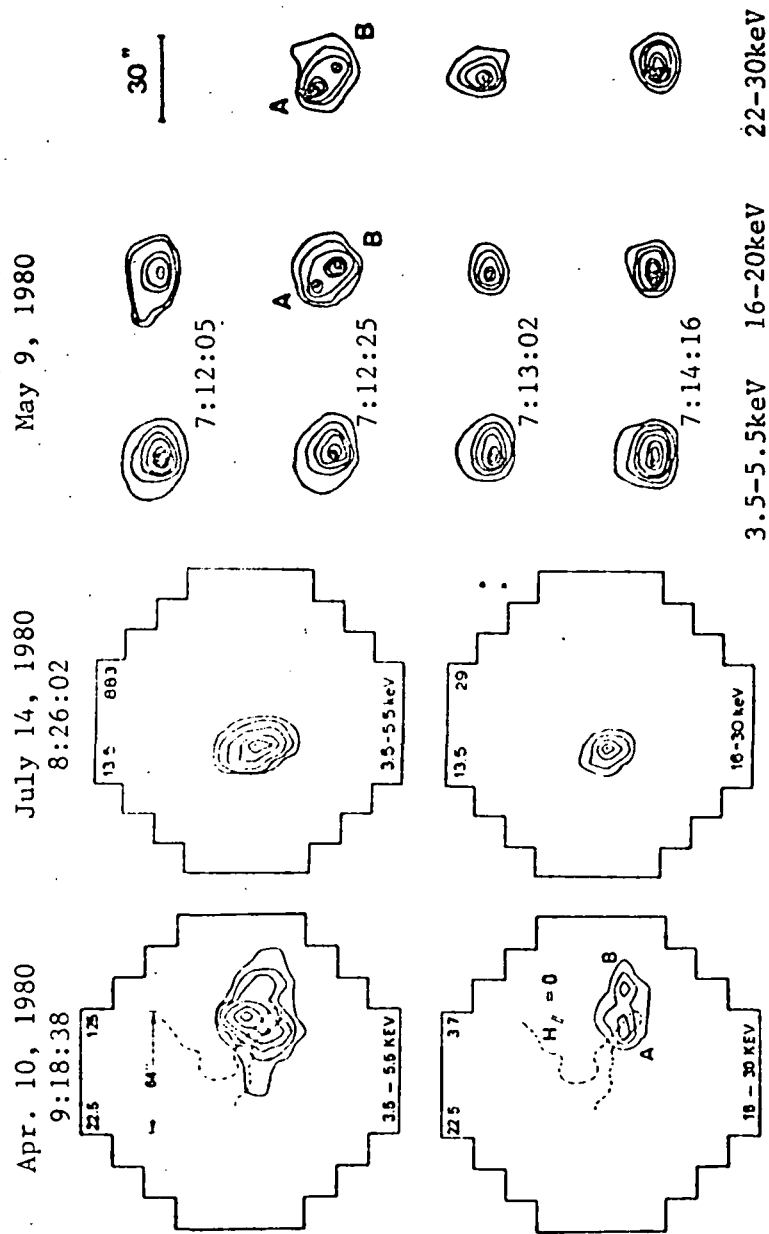


Figure 6

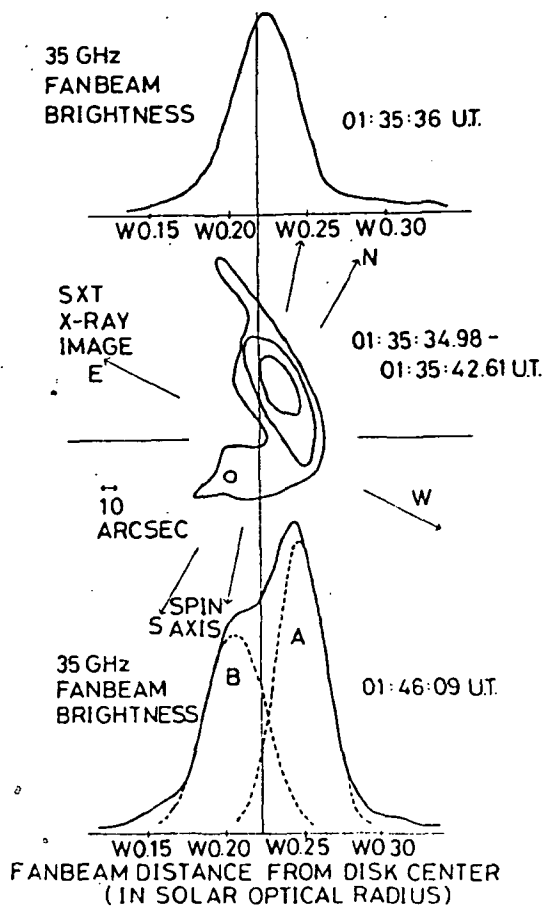


Figure 7

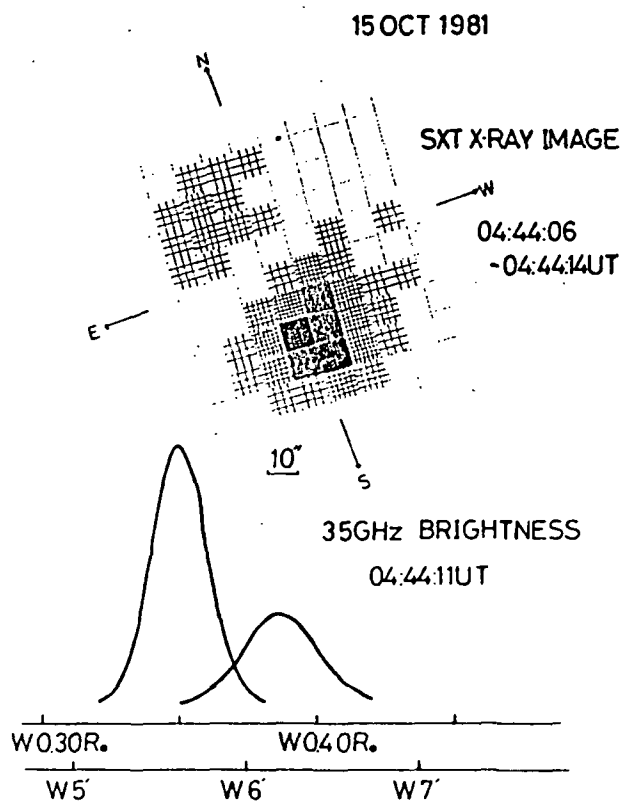


Figure 8

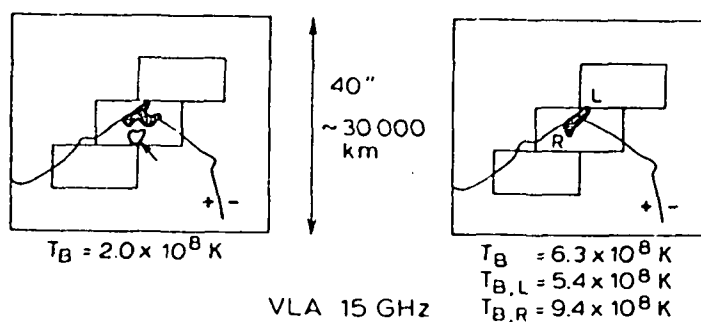


Figure 9

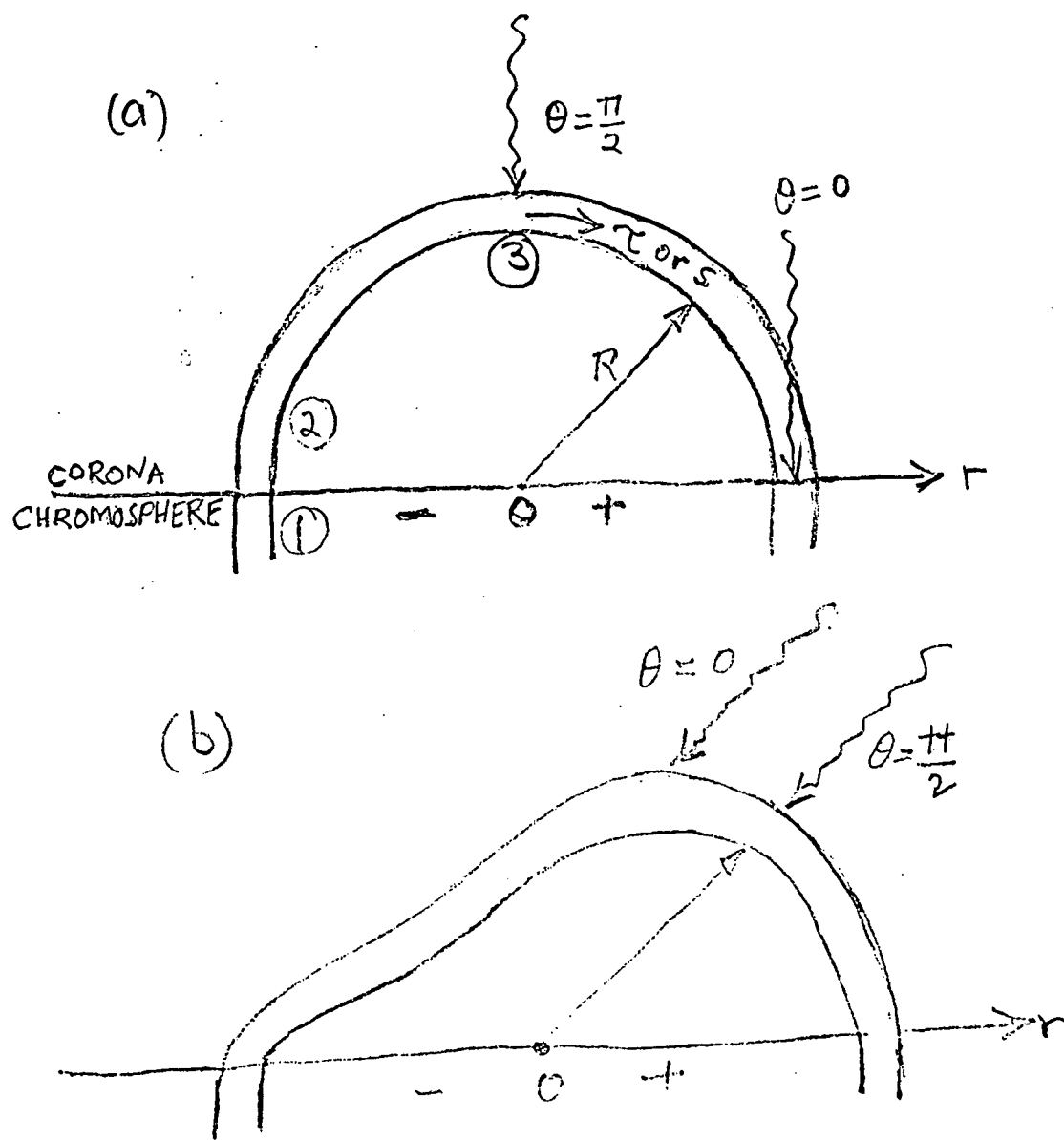


Figure 10

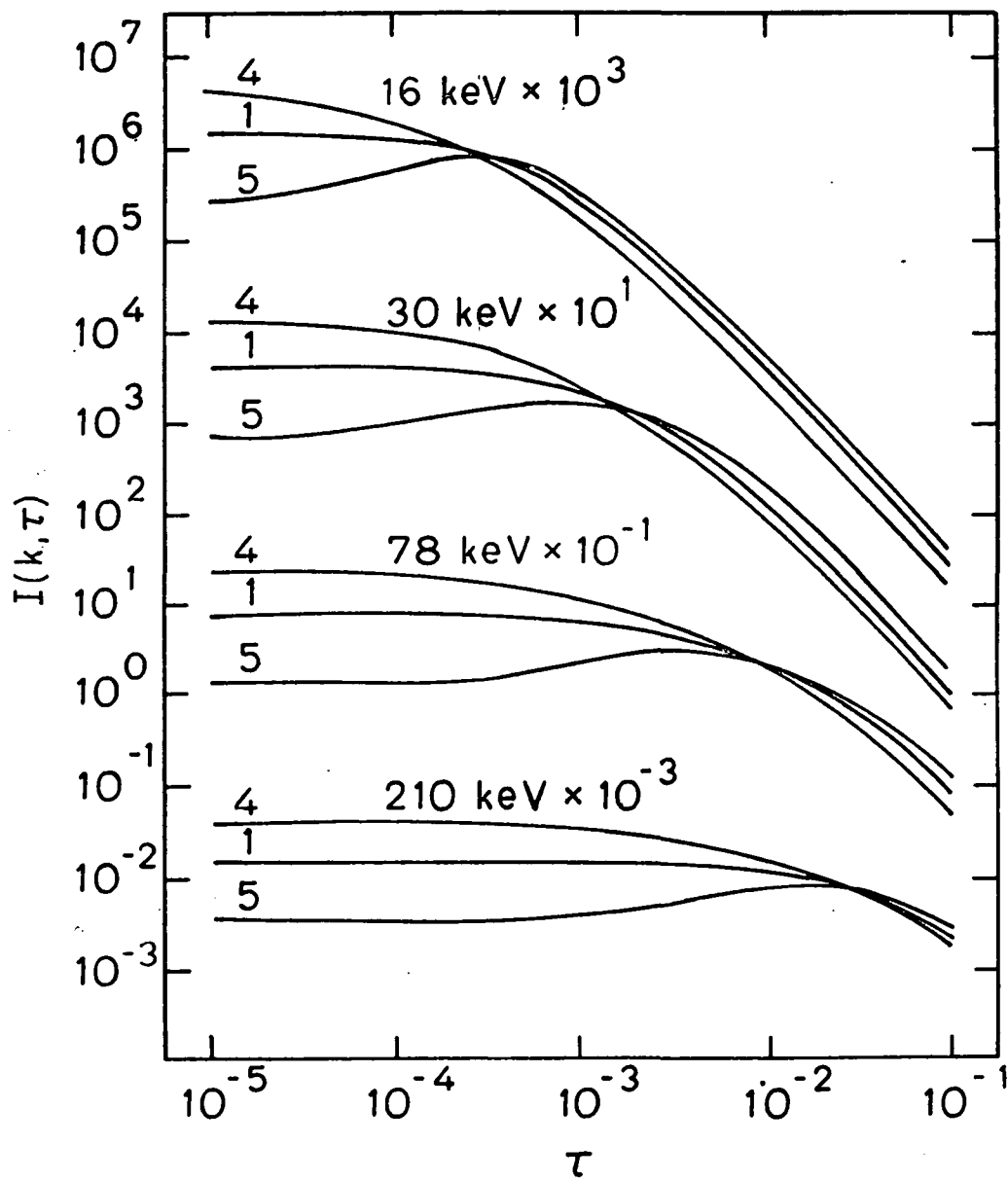


Figure 11

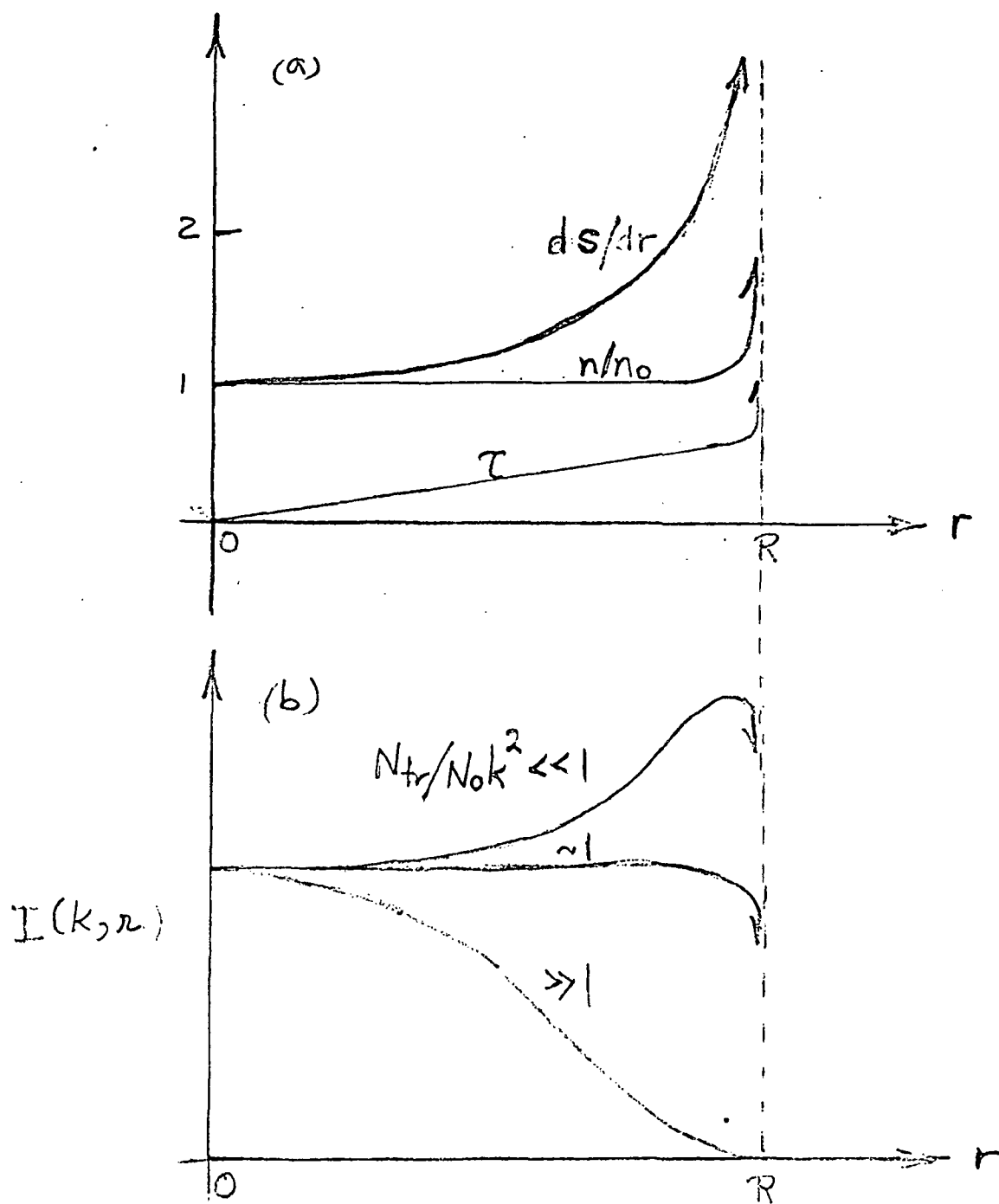


Figure 12

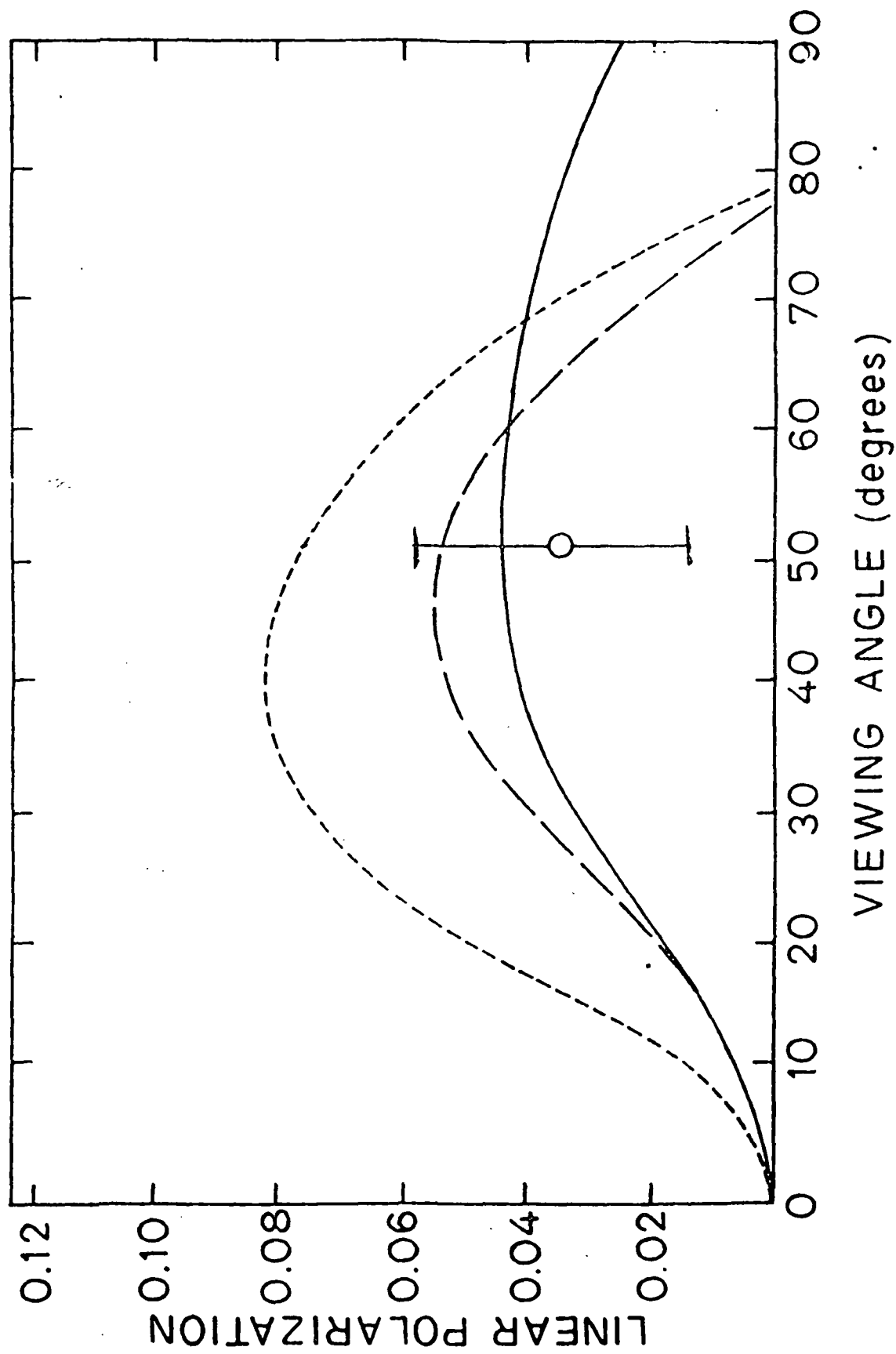


Figure 13